A&A 577, A10 (2015)
DOI: 10.1051/0004-6361/201425076

Astronomy & Astrophysics

Far-infrared study of K giants in the solar neighborhood: Connection between Li enrichment and mass-loss

Yerra Bharat Kumar[1,2], B. E. Reddy[2], C. Muthumariappan[2], and G. Zhao[1]

[1] Key Laboratory of Optical Astronomy, National Astronomical Observatories, Chinese Academy of Sciences, 100012 Beijing, PR China
e-mail: bharat@bao.ac.cn
[2] Indian Institute of Astrophysics, Koramangala II Block, 560034 Bangalore, India

Received 29 September 2014 / Accepted 9 February 2015

ABSTRACT

Context. A small group of red giant branch (RGB) stars are known to have anomalous Li enhancement whose origin is still not well understood. Some studies have proposed that the Li enhancement in RGB stars is correlated to their far-IR excess, a result of mass loss. Studies to confirm such a correlation have a significant bearing on our understanding of the Galactic Li enhancement.
Aims. We searched for a correlation between the two anomalous properties of K giants: Li enhancement and IR excess from an unbiased survey of a large sample of RGB stars.
Methods. A sample of 2000 low-mass K giants with accurate astrometry from the HIPPARCOS catalog was chosen for which Li abundances have been determined from low-resolution spectra. Far-IR data were collected from the WISE and IRAS catalogs. To probe the correlation between the two anomalies, we supplemented 15 Li-rich K giants discovered from this sample with 25 known Li-rich K giants from other studies. Dust shell evolutionary models and spectral energy distributions were constructed using the code DUSTY to estimate different dust shell properties, such as dust evolutionary time scales, dust temperatures, and mass-loss rates.
Results. Among 2000 K giants, we found about two dozen K giants with detectable far-IR excess, and surprisingly, none of them are Li-rich. Similarly, the 15 new Li-rich K giants that were identified from the same sample show no evidence of IR excess. Of the total 40 Li-rich K giants, only 7 show IR excess. Important is that K giants with Li enhancement and/or IR excess begin to appear only at the bump on the RGB.
Conclusions. Results show that K giants with IR excess are very rare, similar to K giants with Li enhancement. This may be due to the rapid differential evolution of dust shell and Li depletion compared to RGB evolutionary time scales. We also infer from the results that during the bump evolution, giants probably undergo some internal changes, which are perhaps the cause of mass-loss and Li-enhancement events. However, the available observational results do not ascertain that these properties are correlated. That a few Li-rich giants have IR excess seems to be pure coincidence.

Key words. infrared: stars – stars: late-type – circumstellar matter – stars: mass-loss – stars: abundances – stars: evolution

1. Introduction

Standard stellar evolutionary models predict severe depletion of Li in red giant branch (RGB) stars owing to convection (Iben 1967a,b). Contrary to expectations, some RGB stars are found to have enhanced Li in their photosphere. Since the discovery of unexpectedly large Li in HD 112127 in 1982 (Wallerstein & Sneden 1982), a number of Li-rich K giants (log ϵ(Li) $\geq$ 1.5 dex) have been found (Hanni 1984; Gratton & D'Antona 1989). However, systematic surveys among RGB stars have shown that the Li-rich K giants are rare, just 1–2% in the Galaxy (Brown et al. 1989; Gonzalez et al. 2009; Kumar et al. 2011; Lebzelter et al. 2012; Monaco et al. 2011; Ruchti et al. 2011) and nearby dwarf spheroidal galaxies (Kirby et al. 2012).

It is important to know whether the Li-rich K giants contribute to the Galactic Li enrichment. Enhancement of the Li abundance from its primordial value, A(Li) $\approx$ 2.27–2.72 dex (Lind et al. 2009; Cyburt et al. 2008), to its present level, A(Li) $\approx$ 3.3 dex (Matteucci 2010), in the Galaxy is clear evidence of Li production in the post-big bang nucleosynthesis. Some of the known sources of Li enhancement in the universe are cosmic ray spallation, supernovae, novae, asymptotic giant branch (AGB) stars (Matteucci 2010, and references therein).

Evidence of the RGB contribution to the Galactic Li enhancement comes in the form of a proposed correlation between Li enhancement and far-IR (FIR) excess in RGB stars (Gregorio-Hetem et al. 1993; de La Reza et al. 1996, 1997; de la Reza & Drake 2012). However, these studies were based on a small number of Li-rich K giants. Most important is that many of the Li-rich K giants discovered in their studies came from the Pico Dias Survey (or PDS), which was meant for finding T Tauri stars based on FIR colors that prompted more surveys to look for Li-rich K giants among IRAS sources (de La Reza et al. 1997; Castilho et al. 1998; Fekel & Watson 1998; Jasniewicz et al. 1999). Obviously, the number of Li-rich K giants with IR excess among K giants has increased (de La Reza et al. 1997; Reddy et al. 2002; Reddy & Lambert 2005).

Like Li-enhancement, IR excess is also unexpected in RGB stars (Zuckerman et al. 1995; Plets et al. 1997). Based on dust shell evolutionary models, de La Reza et al. (1996) suggested that IR excess and a large amount of Li in RGB stars were transient phenomena that would last for a few tens of thousand years. Palacios et al. (2001) provides a mechanism where rotation-induced mixing could cause both the Li-enhancement, as well as mass loss during their evolution of

the RGB luminosity bump. Another interesting study was done by Denissenkov & Herwig (2004) and Carlberg et al. (2010), who suggest that Li enrichment could be due to enhanced extra mixing triggered by external events, such as the plunging of massive planets or by a brown dwarf. According to them, IR excess could be due to a dusty disk orbit around the Li-rich giant (see also, Jura 2003), which might have formed either due to the engulfment of planets or the evaporation of planetesimals (Plets et al. 1997; Jasniewicz et al. 1999). This would mean Li-rich K giants with IR excess could be anywhere on the RGB and not necessarily at the luminosity bump (see Charbonnel & Balachandran 2000; Kumar et al. 2011).

In this paper, we have revisited the problem in light of the increased number of Li-rich K giants that are twice that of the samples involved in the previous studies and the availability of better astrometry and IR data for a large sample of RGB stars. According to our knowledge this is the first uniform study involving a large sample of 2000 low-mass K giants to search for evidence of a connection between the two anomalous properties: Li-enhancement and IR excess.

2. Sample selection and data

Our sample contains 2000 low-mass (0.8–3.0 $M_{\odot}$) K giants in the solar neighborhood ($d \leq 200$ pc), with accurate astrometry (parallaxes and proper motions) taken from the HIPPARCOS Catalog (van Leeuwen 2007). This is the same sample as was used by Kumar et al. (2011) for their search for Li-rich K giants. The sample covers the RGB evolution from its base to well above the RGB bump, spanning the luminosity range from $\log(L/L_{\odot}) \approx 1.0$ to 2.5. In the survey they found 15 new Li-rich K giants (Kumar et al. 2011), 14 of which belong to the thin disk, and one belongs to the thick disk. In addition to 15 new Li-rich K giants, another 25 were included from the literature following the criterion suggested by Charbonnel & Balachandran (2000). The Li abundance data for the entire Li-rich sample was taken from Kumar et al. (2011), Liu et al. (2014), Adamow et al. (2014), and references therein. Of the 25 Li-rich K giants taken from the literature 22 belong to the thin disk component, one to the thick disk component and one to the halo. The status is unknown for the remaining star because kinematic velocities are not available. Li-rich K giants in the sample have solar metallicity within ±0.1 dex.

Owing to the unavailability of astrometry and, in some cases, of IR data, Li-rich K giants from the recent surveys of different populations are not included: Galactic thick disk (Monaco et al. 2011), halo (Ruchti et al. 2011), bulge (Gonzalez et al. 2009; Lebzelter et al. 2012), and dwarf Spheroidal galaxies (Kirby et al. 2012). We did not include Li-rich giants from other studies (Martell & Shetrone 2013; Monaco et al. 2014; Silva Aguirre et al. 2014) for the same reason. The entire survey sample, along with 40 Li-rich K giants, is shown in the Hertzsprung-Russell (HR) diagram (Fig. 1). The sample is superposed on the evolutionary tracks (Bertelli et al. 2008) of masses from 0.8 to 3.0 $M_{\odot}$ with solar metallicity of [Fe/H] = 0.0. Also, shown in Fig. 1 are the base of the RGB (dashed red line) and the region of red clump (black lines) and the luminosity bump (red lines) on each of the mass tracks. Li-rich K giants are shown with symbol size indicating amount of Li abundance.

Infrared data of the entire sample including Li-rich K giants come from the catalogs of the Wide-field Infrared Survey Explorer (WISE; Cutri & et al. 2012, 2013; Wright et al. 2010) and the Infrared Astronomical Satellite (IRAS; Helou & Walker 1988; Kleinmann et al. 1986; Moshir et al. 1990). The

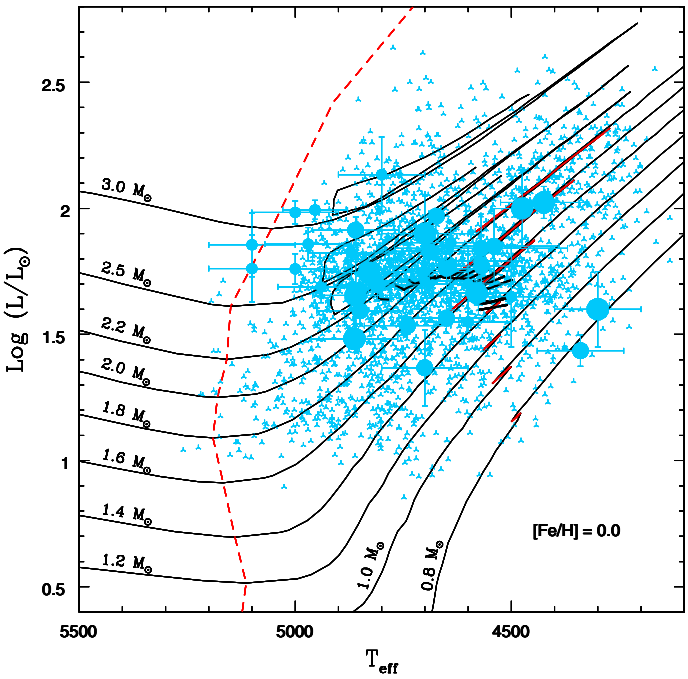

Fig. 1. HR-diagram showing survey sample (crosses) and the Li-rich K giants (filled circles) along with evolutionary tracks for low mass stars (0.8–3 $M_{\odot}$). The size of the circle indicates amount of Li abundance.

IRAS catalog contains flux densities at four different bands with central wavelengths of 12 μm, 25 μm, 60 μm, and 100 μm. The 100 μm flux densities are upper limits for most of the sample stars. For our study, we used only the first three IRAS bands. We divided our sample into three groups: good, moderate, and not good. The group with measured flux densities in all three bands are considered as good, the group with measured flux densities in only two bands are considered as moderate, and the group with measured flux densities only in one band is considered as not good. Of 2000 giants in the sample, we have good IRAS data only for 114 stars and moderate data for 1144 stars. We have used only good and moderate IRAS data in the analysis.

The IRAS data is supplemented by WISE IR flux densities. WISE has four IR bands known as W1, W2, W3, and W4 with central wavelengths at 3.3 μ, 4.6 μ, 11.6 μ, and 22.1 μ, respectively. We used flux densities measured at the W2, W3, and W4 bands. Of 2000 sample stars, 1880 have measured flux densities in all three bands, and all the sample stars have measured flux densities in W3 and W4. All the 40 Li-rich K giants have measured flux densities in W3 and W4 bands, but one star has upper limit flux density in the W2 band. We did not include stars with WISE upper-limit data, which is a very small number any way. Unfortunately, AKARI FIR (65 μ) data (Yamamura et al. 2010) is only available for three stars in our sample. We do not comment any further on this data.

3. Far-IR color–color diagram

Far-IR (FIR) flux excess indicates the presence of circumstellar dust, which can be traced using the FIR color-color diagram (FIR-CCDm). The FIR colors between the two bands with central wavelengths λ_1 and λ_2 were calculated using the following equation:

$$[\lambda_1 - \lambda_2] = \log(\lambda_2 f_{\lambda_1}) - \log(\lambda_1 f_{\lambda_2}) \quad (1)$$

where f_{λ_1} and f_{λ_2} are the flux densities.

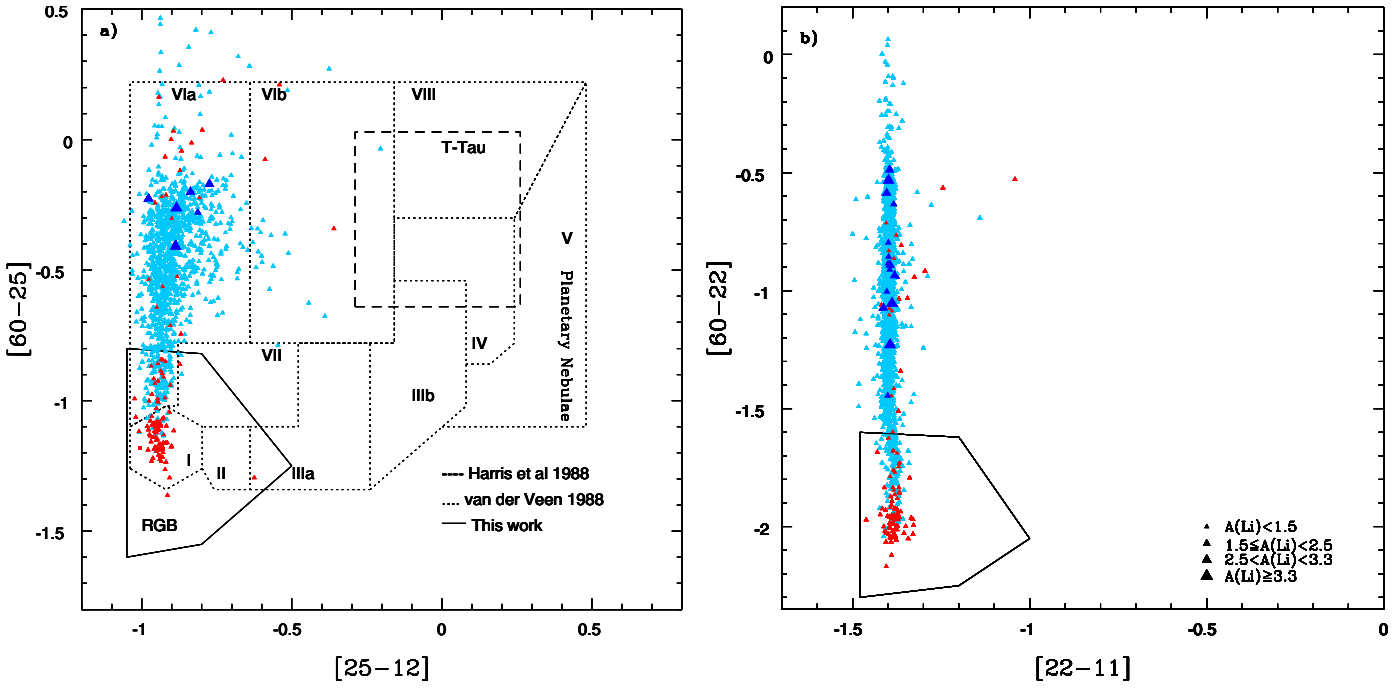

Fig. 2. Sample stars (triangles) shown in FIR color–color diagram. Red and blue colors indicate good and moderate data, respectively. Boxes with dotted lines in Fig. 2a show different phases of dust shell evolution based on the IRAS colors. The box with a dashed line represents a region of young T Tauri stars (Harris et al. 1988). The box with a solid line in both Figs. 2a and b represents the region of RGB stars. Also, shown is Arcturus, a typical K giant (red square). In Fig. 2b, the sample is plotted using WISE 11.6 μ and 22.1 μ and IRAS 60 μ flux densities.

3.1. Survey sample

IRAS colors of the sample stars of good and moderate groups are shown in Fig. 2a, along with Li-rich K giants. Following the study of IRAS data of stars with dust envelopes by van der Veen & Habing (1988), we partitioned the CCDm into different boxes and labeled them accordingly. The Vanderveen diagram is found to be useful tool for interpreting the evolution of dust around the star. For example, Region I represents stars with no dust, and Regions II, IIIa, IIIb, IV, VIb, and VIa represent stars with dust going progressively from warm to cool. Photospheric far-IR colors of RGB stars with no IR excess are represented by Region RGB (see Fig. 2a). As shown in Fig. 2a, most of the stars are in Region RGB and VIa, and a very few are in other regions. Of the stars with good data, the majority are in Region RGB with no excess of dust. A few are in Regions VIa and VIb. However, the vast majority of stars with moderate data are in Region VIa. This could be due to 60 μm flux density, which is an upper limit. We assume that all of these stars belong to Region RGB with no excess of dust. We note that only a small fraction of stars with good data show detectable far-IR excess, which confirms the earlier estimation of far-IR excess among the giants of luminosity class III (see Zuckerman et al. 1995; Plets et al. 1997).

A similar diagram is shown in Fig. 2b for two WISE measurements at 11.6 μ (W3) and 22.1 μ (W4) and IRAS 60 μ flux density. We have WISE measured flux densities of [22–11] for 1880 sample stars, including all the 15 Li-rich K giants from the sample against IRAS measured flux densities of [25–12] for 1144 sample stars. WISE colors [22–11] show much less scatter and show excess for very few stars. Also, none of the 15 Li-rich K giants show excess in [22–11] and fall in the same region as normal K giants, confirming the IRAS data based on a relatively small number of measured flux densities.

3.2. Li-rich K giants

We have a total of 40 Li-rich K giants, 15 of which come from our survey (Kumar et al. 2011), and the rest are from the literature. All of them are shown in Fig. 3a of IRAS CCD. Arcturus, a typical K giant with very low Li (A(Li) ~ -0.6) and no IR excess, is shown as a reference. The IRAS data and colours of 40 Li-rich K giants are given in Table 1. Of 40 Li-rich K giants, 7 have "good data", 18 have "moderate data", and another 15 have "not good data". Unfortunately, none of the 15 Li-rich K giants found from our survey of 2000 K giants belong to the good data group. However, six of them have measured flux densities in 12 μ and 25 μ and fall in the region VIa. From Fig. 3a, we note only 7 Li-rich K giants showing IR excess in both 25 μ and 60 μ bands, suggesting clear evidence of a dust envelope and of the recent mass loss. For 18 stars with moderate data, flux densities of 12 μ and 25 μ bands are normal and show no evidence of excess flux. However, [60–25] color indicates cool dust (region VIa), but this may be entirely due to the upper limit in 60 μ flux. These candidates most likely show black-body [25–12] color of their photospheres, and at 60 μ the photospheric flux densities are too faint to be detected. The third group (black symbols) have only upper limit flux densities both in 25 μ and 60 μ and would be difficult to say whether they have or do not have IR excess.

However, WISE measured flux densities at 22.1 μ and 11.6 μ are available for all 40 Li-rich K giants. The good quality of IRAS 60 μ flux densities are available for only seven Li-rich K giants, and the rest are with upper limits. In Fig. 3b, we showed all the 40 Li-rich K giants in the plot of [22–11] and [60–22] color. It is clear from the figure that stars that have measured flux densities in all three bands are the same seven Li-rich K giants that show IR excess indicating some kind of warm dust. The position of black symbols in Fig. 3a moved to the left in Fig. 3b, showing no IR excess in [22–11] color. Since 60 μ flux

Table 1. IRAS flux densities and Li abundances of Li-rich giants.

Star	A(Li)	F12 (Jy)	Quality	F25 (Jy)	Quality	F60 (Jy)	Quality	[25–12]	[60–25]	Reference
HD 183492	2.07	2.377	2	2.512	1	0.8849	1	−0.294	−0.833	3
HD 107484	2.14	0.410	3	0.156	1	0.298	1	−0.738	−0.099	7
HD 108471	2.10	0.869	3	0.361	1	0.4	1	−0.700	−0.335	3
HD 118319	2.02	1.04	3	0.287	1	0.4	1	−0.877	−0.236	7
HD 120602	2.07	1.129	3	0.278	1	0.4	1	−0.927	−0.222	3
HD 8676	3.55	0.319	3	0.188	1	0.140	1	−0.548	−0.508	7
HD 12203	2.08	0.793	3	0.409	1	0.4	1	−0.606	−0.389	7
HD 133086	2.14	0.706	3	0.25	1	0.4	1	−0.769	−0.176	7
HD 6665	2.93	0.292	3	0.192	1	0.163	1	−0.501	−0.451	13
HD 217352	2.65	0.701	3	0.308	1	0.4	1	−0.675	−0.266	13
HD 63798	2.00	0.865	3	0.347	1	0.4	1	−0.715	−0.318	10
HD 88476	2.21	0.638	3	0.29	1	0.4	1	−0.661	−0.240	7
HD 150902	2.65	0.298	3	0.25	1	0.4	1	−0.396	−0.176	7
HD 37719	2.71	0.376	3	0.25	1	0.4	1	−0.496	−0.176	7
HD 40168	1.70	0.759	3	0.25	1	0.4	1	−0.801	−0.176	7
HD 203136	2.34	0.444	3	0.305	1	0.584	1	−0.482	−0.098	13
TYC3105-00152-1	2.86	0.0602	3	0.0510	1	0.0806	1	−0.391	−0.181	1
HD 112127	2.95	0.979	3	0.290	2	0.4	1	−0.846	−0.241	14
HD 40827	2.05	1.51	3	0.368	2	0.4	1	−0.931	−0.343	3
HD 170527	3.12	0.873	3	0.264	2	0.4	1	−0.837	−0.200	7
HD 51367	2.60	0.705	3	0.246	2	0.4	1	−0.774	−0.170	7
HD 10437	3.48	1.12	3	0.304	2	0.4	1	−0.884	−0.261	7
HD 212430	1.83	1.81	3	0.385	2	0.4	1	−0.991	−0.364	9
HD 102845	1.98	1.08	3	0.207	2	0.4	1	−1.036	−0.094	9
HD 145457	2.49	0.988	3	0.316	3	0.4	1	−0.813	−0.278	7
HD 167304	2.85	1.28	3	0.281	3	0.4	1	−0.977	−0.226	7
HD 214995	2.95	1.84	3	0.438	3	0.4	1	−0.942	−0.419	8
HD 90633	2.18	1.41	3	0.346	3	0.4	1	−0.928	−0.317	10
HD 148293	2.16	3.52	3	0.78744	3	0.4	1	−0.969	−0.674	3
HD 116292	1.50	2.51	3	0.661	3	0.4	1	−0.898	−0.598	3
HD 9746	3.44	2.74	3	0.712	3	0.4	1	−0.904	−0.630	3
HD 77361	3.80	1.58	3	0.427	3	0.4	1	−0.886	−0.408	7
HD 194937	3.18	1.51	3	0.440	3	0.4	1	−0.855	−0.420	8
IRAS 17596-3952	2.30	0.482	3	1.11	2	0.637	2	0.044	−0.621	12
HD 19745	3.40	0.332	3	0.777	3	0.612	3	0.050	−0.483	12
IRAS 13539-4153	3.90	0.491	3	0.821	3	0.644	3	−0.095	−0.485	12
IRAS 13313-5838	3.13	1.88	3	6.04	3	3.3	2	0.188	−0.642	4
PDS100	2.40	4.74	3	6.53	3	3.38	3	−0.179	−0.666	11
HD 219025	2.93	17.1	3	10.3	3	3.86	3	−0.538	−0.806	5, 6
HD 233517	3.95	0.502	3	3.6	3	7.6	3	0.536	−0.055	2

Notes. 1 = Upper limits; 2 = moderate; 3 = high.

References. (1) Adamow et al. (2014); (2) Balachandran et al. (2000); (3) Brown et al. (1989); (4) Drake et al. (2002); (5) Fekel & Watson (1998); (6) Jasniewicz et al. (1999); (7) Kumar et al. (2011); (8) Luck & Heiter (2007); (9) Liu et al. (2014); (10) Mishenina et al. (2006); (11) Reddy et al. (2002); (12) Reddy & Lambert (2005); (13) Strassmeier et al. (2000); (14) Wallerstein & Sneden (1982).

densities are upper limits, we assume that all the Li-rich K giants represented in blue are similar to normal K giants with expected photospheric fluxes. Also, in Fig. 4 we showed WISE colors for the entire sample (1880) and 39 Li-rich K giants excluding stars with upper limits. This too confirms the above findings.

4. Modeling of circumstellar envelope: DUSTY

We used a 1D radiative transfer code, DUSTY (Ivezic et al. 1999), to model the observed spectral energy distribution (SED) and to reconstruct the IRAS color–color diagram with dust evolutionary models. DUSTY solves radiative transport through a dusty region in the circumstellar environment. The solution is obtained through an integral equation for the spectral energy density. DUSTY can handle the geometry of the regions that are plane parallel or spherical density distribution heated by a central source. It has built-in optical constants for most of the astronomical dust grains.

4.1. Spectral energy distribution (SED)

Modeling of SED, constructed from far-UV to the sub-mm data of dust shells around cool giants, is one of the important diagnostic tools for understanding the nature of the dust. To construct the SED, we took optical (*BVRI*; Monet et al. 2003), near-IR (JHK_s) magnitudes (Skrutskie et al. 2006), and FIR (IRAS, WISE) flux densities (Helou & Walker 1988) from the respective catalogs and SIMBAD. Mid-IR fluxes observed by MSX (Egan et al. 2003) were taken wherever applicable. Magnitudes are converted to fluxes (see Bessell et al. 1998; Cohen et al. 2003). The model SED is fitted to the observed SED by scaling the K band model flux to the observed value. In the modeling of dust envelope we used only measured fluxes, not the fluxes with upper limits.

DUSTY computes SEDs for a given set of input parameters: dust temperature at the inner shell (T_d), optical depth (τ) at 0.55 μ, the relative shell thickness (R_{out}–R_{in})/R_{in}, and the

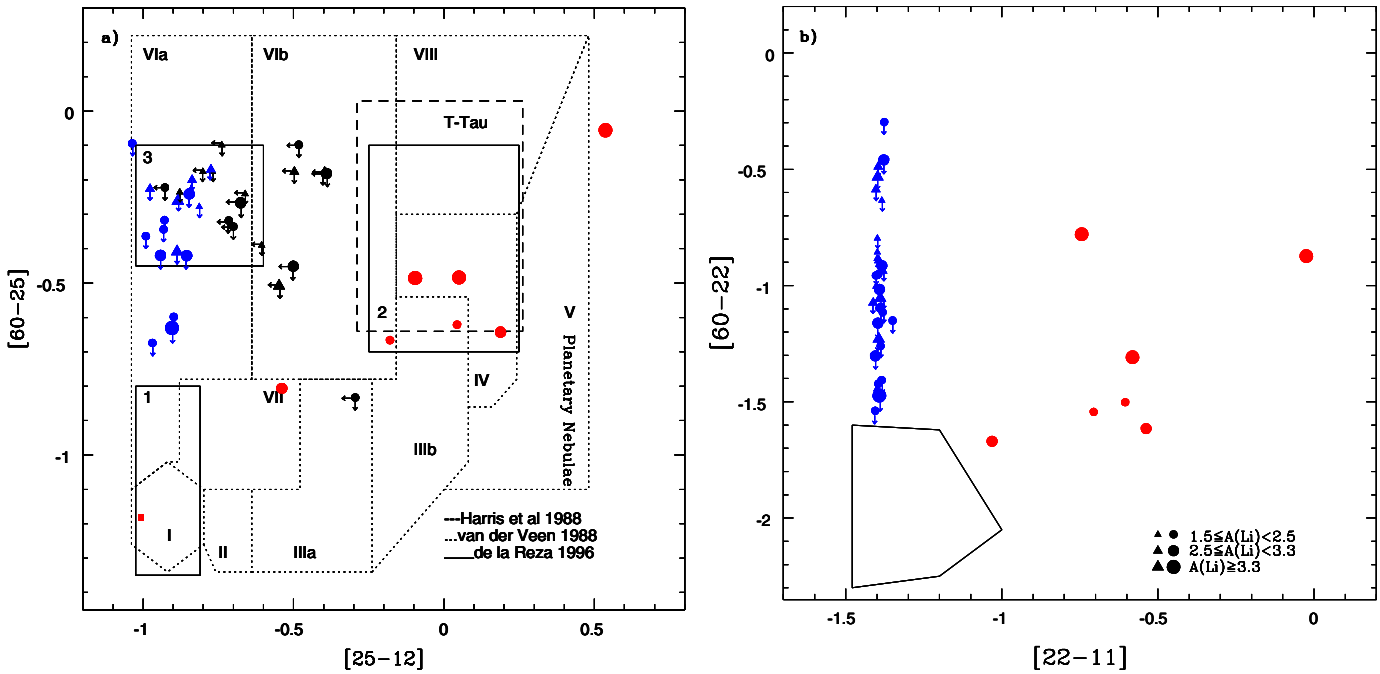

Fig. 3. Location of Li-rich giants in the IR color–color diagram based on only IRAS flux densities (Fig. 3a) and flux densities taken from both WISE and IRAS (Fig. 3b). Li-rich giants from this survey are shown in triangles, and those from other studies are shown as circles. Red, blue, and black colors indicate good, moderate, and not good data, respectively. The size of the symbols represents the amount of Li, $1.5 \leq A(\mathrm{Li}) < 2.5$, $2.5 \leq A(\mathrm{Li}) < 3.3$, and $A(\mathrm{Li}) \geq 3.3$. The red square denotes the Arcturus, a typical K giant with $A(\mathrm{Li}) < 0.0$.

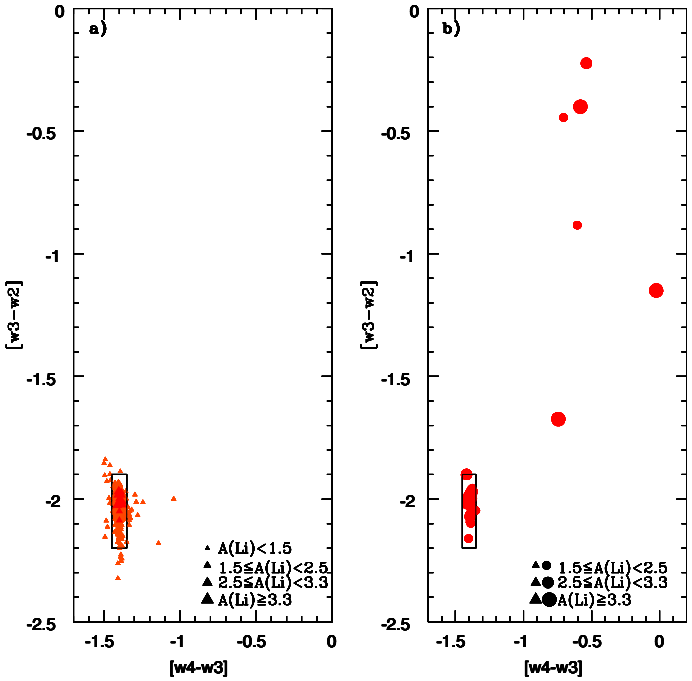

Fig. 4. Location of survey sample and Li-rich giants on the WISE color–color diagram. The Li-normal and Li-rich sample from this survey are shown as red triangles in the *left panel*. 39 Li-rich giants are shown in the *right panel*.

input SED of the central star. The central star was taken as a point source with a spherically distributed dust. To compute the SED for a central star, we have used appropriate model atmospheres from a Kurucz grid of model atmospheres (Kurucz 1994). Atmospheric parameters ($T_{\rm eff}$, log g, and [Fe/H]) were taken from Kumar et al. (2011). The dust shell was assumed to have astronomical silicate grains because most of the RGB stars are oxygen-rich (C/O $\leq$ 1.0). The dust temperature at the inner shell, optical depth, and relative shell thickness were found by an iterative method until the theoretical SED matched the observed SED well. We found that the excess emission was reproduced well with the warm silicate dust grains (Ossenkopf et al. 1992). Derived dust temperatures ($T_{\rm d}$) along with the atmospheric parameters for Li-rich giants with good data are given in Table 2.

4.2. Mass-loss rates and envelope kinematic age

Dust parameters derived from modeling SEDs are used to derive mass-loss rates and kinematic age. Assuming a constant velocity ($V_{\rm s}$) of 2 km s^{-1} for the wind, the rate of mass loss and kinematic age (t) of the dust shell are estimated following de La Reza et al. (1996):

$$\dot{M} = 7.9 \times 10^{-28} \tau_{\rm v} R'_{\rm in} V_{\rm s}; \quad t = \frac{R'_{\rm in}}{V_{\rm s}} \tag{2}$$

where $\tau_{\rm v}$ is the optical depth at visible band, $R'_{\rm in}$ is inner dust shell radius. The derived values for the seven Li-rich K giants with good data are given in Table 2.

Furthermore, we predicted mass loss rates of RGB stars at different phases in their evolution. In Table 3, we have provided expected mass-loss rates. The mass-loss rates are computed using the modified version of the Reimer's law (Schröder & Cuntz 2005; $\dot{M}_{\rm R}$):

$$\dot{M}_{\rm R} = \frac{\eta L_\star R_\star}{M_\star} \left(\frac{T_{\rm eff}}{4000}\right)\left(1 + \frac{g_\odot}{4300 g_\star}\right) \tag{3}$$

where $\eta = 8 \pm 1 \times 10^{-14}\ M_\odot\ \mathrm{yr}^{-1}$; $L_\star$, $R_\star$, $M_\star$, $g_\star$ are luminosity, radius, mass, and surface gravity of a given star, respectively. For

Table 2. Photospheric and dust parameters of Li-rich K giants with IR excess.

Star	[Fe/H]	$T_{\rm eff}$ (K)	$\log g$	$\mathrm{Log}(L/L_\odot)$	$R/R_\odot$	$\dot{M}$ ($M_\odot\,\mathrm{yr}^{-1}$)	$T_{\rm dust}$ (K)	t (yr)
HD 233517	−0.37	4475	2.25	2.00	16.6655	1.88577E-07	75	1262.99
HD 219025	−0.10	4570	2.30	1.88	13.9179	6.02185E-09	275	40.3312
HD 19745	−0.05	4700	2.25	1.90	13.4651	3.50690E-09	170	117.437
IRAS 13539-4153	−0.13	2.25	4300	1.60	11.3885	3.27951E-08	230	47.0666
IRAS 17596-3952	0.10	2.50	4600	1.70	11.1658	2.37905E-08	190	85.3588
IRAS 13313-5838	−0.09	2.20	4540	1.85	13.6236	1.29749E-07	260	46.553
PDS 100	0.14	4500	2.50	1.70	11.6676	1.48663E-08	250	29.87

Table 3. Expected Reimers' law mass-loss rates at different locations on RGB.

Bin	$T_{\rm eff}$ (K)	$\log(L/L_\odot)$	$M_\star$ ($M_\odot$)	$R_\star$ ($R_\odot$)	$\log g$	$\dot{M}_{\rm R}$ ($M_\odot\,\mathrm{yr}^{-1}$)
Prebump	4650	0.9	1.0	4.3501	3.163	4.83757E-12
	4650	1.5	1.6	8.67958	2.76712	2.40163E-11
	5200	1.0	1.9	3.903	3.53596	2.87589E-12
	5200	1.5	2.5	6.94062	3.15514	1.2291E-11
	4800	1.3	1.8	6.47027	3.07343	1.0041E-11
Bump	4500	1.0	0.8	5.2117	2.90913	9.12048E-12
	4500	1.6	1.2	10.3987	2.48522	4.82977E-11
	4650	1.0	1.0	4.88089	3.063	6.83324E-12
	4650	2.0	2.5	15.4347	2.46094	8.64344E-11
	4200	2.0	0.8	18.9193	1.78928	3.31089E-10
	4600	1.75	1.8	11.8274	2.54949	5.17303E-11
Clump	4650	1.5	1.4	8.67958	2.70913	2.74472E-11
	4650	2.0	2.2	15.4347	2.40543	9.8221E-11
	5000	1.5	2.5	7.50697	3.08701	1.32939E-11
	5000	2.0	3.5	13.3495	2.73314	5.3398E-11
	4750	1.75	2.3	11.0922	2.71169	3.7968E-11
Postbump	4200	2.0	1.0	18.9193	1.88619	2.64871E-10
	4200	2.5	2.1	33.6439	1.70841	7.09275E-10
	5000	2.0	3.0	13.3495	2.66619	6.22976E-11
	4800	2.4	4.0	22.9574	2.32022	2.01832E-10
	4300	2.1	1.8	20.252	2.08234	1.983E-10
	4500	2.2	2.5	20.7482	2.20398	1.84148E-10

solar gravity, $\log g_\odot = 4.44$ has been adopted. Radii for the stars are calculated from their luminosities and temperatures. Stellar gravities ($\log g_\star$) have been derived using the following standard equation:

$$\log g = \log \frac{L}{L_\odot} + \log \frac{M}{M_\odot} + 4 \log T_{\rm eff} - 10.61. \quad (4)$$

The expected mass-loss rates of normal giants are in the range of 10^{-12} to 10^{-10} $M_\odot\,\mathrm{yr}^{-1}$, which are one to two orders of magnitude lower than the observed values of Li-rich K giants with far-IR excess (Tables 2 and 3).

4.3. Circumstellar dust shell evolutionary model

In Fig. 5, DUSTY-computed far-IR colors are shown for a set of stellar parameters covering RGB evolution. For computation, we assumed that the dust shell is spherically symmetric, thin, and detached from the central star and that it is a uniform mixture of dust and gas. We also assumed that the newly formed dust shell is a result of uniform mass loss, hot with $T_{\rm d} = 1500$ K (sublimation temperature of silicates) and cooling down to $T_{\rm d} = 15$ K (dust temperature of diffuse interstellar medium) before it dissipates into the interstellar medium. In computing the dust shell evolution, we considered four different mass-loss rates: 1×10^{-10}, 1×10^{-9}, 5×10^{-9}, and 3×10^{-8}.

5. Discussion

From the survey, we found only 114 K giants with measured flux densities in all three IRAS (12 μ, 25 μ, and 60 μ) bands. Of these only 23 show evidence of far-IR excess due to cold dust (regions V1a, VIb), and the rest have no excess of dust (region RGB; see Fig. 2a). Interestingly, none of these K giants with far-IR excess are Li-rich. Similarly, only 15 out of the 2000 K giants are Li-rich (see Kumar et al. 2011), and none of them show evidence of far-IR excess. For many stars in the sample, only IRAS upper limits are available for both 12 μ and 25 μ. To improve the situation we supplemented IRAS data with WISE data that has measured flux densities for almost all the stars in 11.6 μ and 22.1 μ. The combined IRAS and WISE data results suggest that the far-IR excess among K giants is uncommon, which confirms earlier results by Zuckerman et al. (1995) and Plets et al. (1997). This may be due to the fast depletion of enhanced Li and dust dissipation in an uncorrelated way. Important is that the unbiased survey results do not confirm earlier suggestions (de La Reza et al. 1996, 1997) of a correlation between the two anomalous properties of K giants: Li-enhancement and far-IR excess.

To gain more insight, we included 25 Li-rich K giants from the literature. These are shown in Fig. 3a along with 15 (black & blue triangles) Li-rich K giants from the present survey. Of 40, only 7 have measured flux densities in all the three IRAS (12 μ,

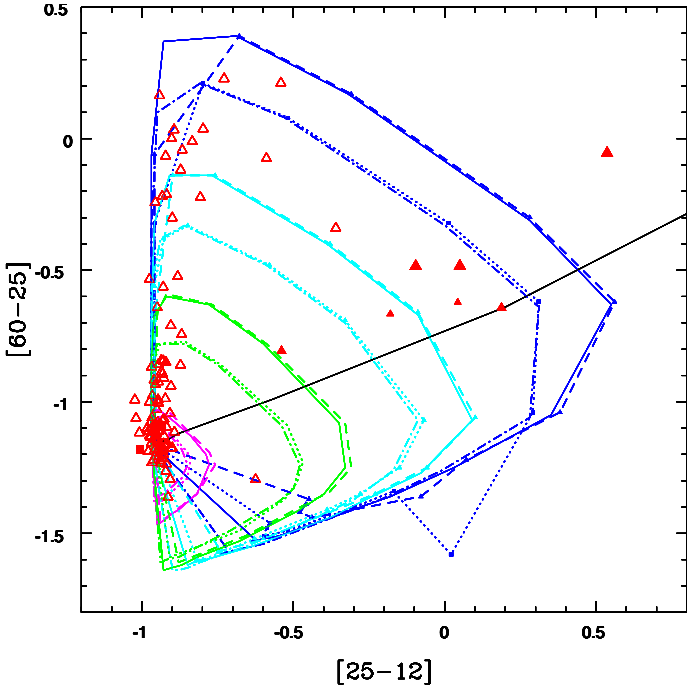

Fig. 5. Li-rich (filled triangles) and Li-normal (open triangles) giants with good quality data are superposed with dust shell evolutionary models. Different colors; magenta, green, cyan, and blue represent the loops of the evolution of a dust shell with mass-loss rates, 1×10^{-10}, 1×10^{-9}, 5×10^{-9}, and 3×10^{-8}, respectively. Four varieties of lines in each color indicate the different photospheric temperatures and radius, $T_{\rm eff}$ = 5000 K, R = 20 $R_{\odot}$, $T_{\rm eff}$ = 4000 K, R = 20 $R_{\odot}$, $T_{\rm eff}$ = 5000 K, R = 10 $R_{\odot}$, $T_{\rm eff}$ = 4000 K, R = 10 $R_{\odot}$ of the dust shell hosting stars, radially outward, respectively.

Table 4. Dust parameters and evolutionary timescales for different photospheric parameters of RGB stars

$\dot{M}$ ($M_{\odot}$ yr^{-1})	$T_{\star}$ (K)	$R_{\star}$ ($R_{\odot}$)	$T_{\rm dust}$ (K)	Age (yr)
1×10^{-10}	4000	10	25	16 548
		20	28	23 641
	5000	10	27	37 802
		20	31	50 164
1×10^{-9}	4000	10	17	52 163
		20	19	74 736
	5000	10	19	107 675
		20	20.5	171 636
5×10^{-9}	4000	10	15	75 957
		20	16	125 070
	5000	10	15.5	198 868
		20	17	300 273
3×10^{-8}	4000	10	13	116 681
		20	13.5	208 958
	5000	10	13.5	299 198
		20	14	53 7481

Table 5. Evolutionary timescales from the RGB bump to the red clump.

$M_{\star}$ ($M_{\odot}$)	$t_{\rm bump}$ (yr)	$t_{\rm bump-tip}$ (yr)	$t_{\rm clump}$ (yr)
1.0	1.52E+07	1.27E+08	9.49E+07
1.2	1.11E+07	9.87E+07	7.98E+07
1.4	8.12E+06	7.50E+07	7.61E+07
1.6	6.85E+06	5.68E+07	8.07E+07
1.8	4.07E+06	3.54E+07	9.17E+07
2.0	2.45E+06	1.95E+07	1.03E+08

25 μ, and 60 μ) bands, and show evidence of warm dust. Among seven super Li-rich K giants (log ϵ Li $\geq$ 3.3) in the sample only three show IR excess and all the three have been selected based on IR colours. Important is that four other super Li-rich K giants show no evidence of IR excess, certainly no warm dust around giants with such high Li (Fig. 3b). This observational result contradicts the hypothesis (de La Reza et al. 1996, 1997) that the evolution of Li abundance and IR excess are correlated wherein the larger the Li abundance in K giants, the hotter the circumstellar dust, the less the Li abundance, and the cooler the circumstellar dust. The large Li abundance in K giants implies recent enhancement of Li accompanied by a mass-loss event (hence the warm dust), suggesting that not much time has elapsed since the events that caused Li enhancement and dust shell ejection.

Results from dust models, shown in Fig. 5 and Table 4, suggest that the dust evolutionary time scales are quite small at a few thousand to a few hundred thousand years for typical K giants with the least mass loss rates (1×10^{-10}) to heavy mass loss rates (5×10^{-8}), respectively. Also, Li-depletion timescales, according to Li Flash model (Palacios et al. 2001), are on the order of 10^4 ($\approx$20 000) yrs. These time scales are much smaller than stellar evolutionary time scales (Bertelli et al. 2008) and, important, smaller than the evolutionary timescales of different phases along the RGB (see Table 5). K giants spend a few million years ($t_{\rm bump}$) at the bump and take about 10–100 million years to evolve from the bump to the clump via the tip of the RGB. The above arguments suggest that the ejected dust shell due to mass loss and the enriched Li may not even survive the bump evolution. It is still an open question whether it is just a coincidence that seven Li-rich K giants have been found to have far-IR excess (Figs. 3a, b) or that these two properties are somehow related but not observed owing to their fast but different evolutionary scales. To understand the later question, we plotted the entire sample along with the 40 Li-rich K giants in the HR diagram (Fig. 6). Results shown in Fig. 6 complicate the situation further. From close examination of the displayed data, one could make a few interesting observations: a) there seem to be two groups of Li-rich K giants: one at the luminosity bump and another at the clump; b) the Li-rich K giants that overlap with the clump region (just below the bump and to the left) do not show far-IR excess; c) some of the Li-rich K giants in the bump region show far-IR excess due to warm dust; d) we note that the K giants with far-IR excess and/or Li-enhancement occur in the narrow luminosity range (log($L/L_{\odot}$) = 1.4–2.2).

The absence of Li-rich K giants below the bump suggests that Li production begins during the bump evolution. Interestingly, the K giants with far-IR excess also begin to appear at or within the bump region. In fact, all seven Li-rich K giants with far-IR excess are in the bump region (Fig. 6). However, within the same region, there are also Li-rich giants without far-IR excess and far-IR excess K giants without Li enhancement. Thus, one ought to be cautious about associating Li-enhancement in K giants with the mass-loss events or vice versa. Also, assuming the possibility that planet engulfment enriches host-star Li abundance, hence IR excess (see Denissenkov & Herwig 2004; Carlberg et al. 2010; Adamow et al. 2014), and that the engulfment may happen anywhere along the RGB, one would expect Li enhancement across the RGB but not necessarily at the narrow bump luminosity. Absence of K giants with Li enhancement below and above the bump region casts shadow on the external origin scenario.

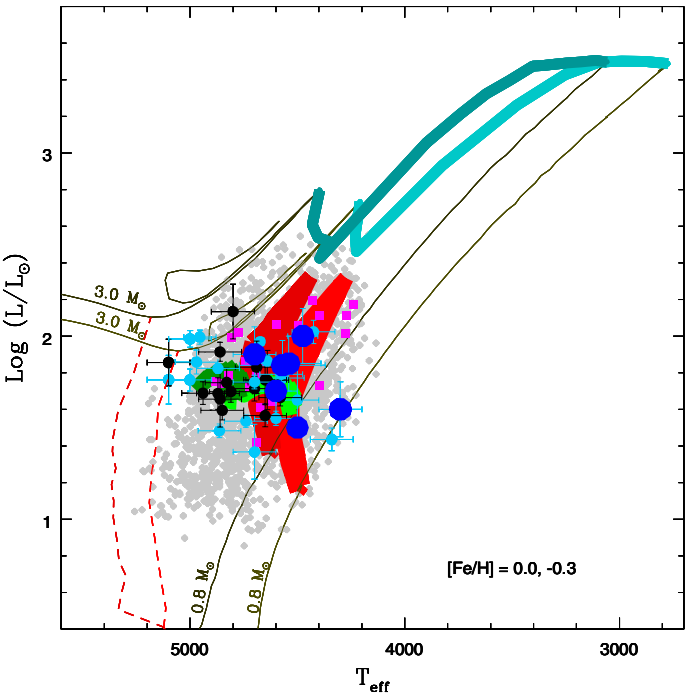

Fig. 6. Li-rich K giant sample (circles) and K giants with IR excess (squares) in the HR diagram. Evolutionary phases: RGB base (broken lines), luminosity bump (red shade), RGB tip (blue band), clump region (green shade) are shown. The 15 Li-rich K giants taken from Kumar et al. (2011) are shown as black circles and the rest as light blue circles. K giants with both far-IR excess and Li enhancement are shown as big blue circles. Tracks of K giants with mass 0.8 $M_{\odot}$ and 3.0 $M_{\odot}$ are shown. All the evolutionary phases are shown for two metallicity values of [Fe/H] = 0.0 and −0.3.

The presence of Li-rich and also super Li-rich K giants without far-IR excess (blue triangles in Fig. 3a, box 3) at the clump (see green shade in Fig. 6) requires an alternative site for Li enhancement, other than the bump. It is very unlikely that the Li produced at the bump remains at its peak value. As giants evolve to the clump via the tip of the RGB they experience deep convection. The extent of mixing is evidenced by their very low values of $^{12}C/^{13}C$ ratios (see Kumar & Reddy 2009; Kumar et al. 2011). Thus, in Kumar et al. (2011) study core-He flash at the tip of the RGB has been suggested as the most likely alternative event that could cause Li enhancement that might or might not have been associated with the mass loss. Since the evolution from the tip of the RGB to the clump is rapid, Li produced at the tip is expected to survive. However, in a recent study by Denissenkov (2012), an alternative scenario was proposed in which, as a result of extra-mixing, giants originated in the bump could make extended zigzags that may reach luminosities below the bump luminosity explaining a group of Li-rich K giants that appear to overlap with the red clump in the HR diagram (Fig. 6).

6. Conclusion

We performed a search for a correlation between Li-enhancement and far-IR excess among a uniform sample of 2000 K giants. Infrared data for the sample is taken from the WISE and IRAS catalogs. Results suggest that IR excess similar to Li enhancement among the K giants is uncommon. Results from the survey show no direct evidence of correlation between the two anomalous properties of K giants. None of the 15 Li-rich K giants show IR excess, and none of the K giants that have measurable IR excess show Li enhancement.

Furthermore, Li-rich K giants from the survey are supplemented by 25 known Li-rich K giants from different studies. Absence of Li-rich and/or IR excess K giants below the bump stresses the fact that K giants undergo some key internal changes during the short span of bump evolution leading to mass loss and Li enhancement. Though the evidence for the two events occurring during the bump are clear from our study, what is not clear is whether one phenomenon triggers another, leading to a correlation, or whether the two events are independent. Results from our observations and from the compilation of Li-rich K giants favor the later suggestion. The presence of both IR excess and Li enhancement in a few K giants seems to be a coincidence.

To get a better perspective on the problem, it is important to search for Li enhancement among red clump stars and RGB bump stars separately. Also, several studies (Gonzalez et al. 2009; Monaco et al. 2011; Lebzelter et al. 2012; Ruchti et al. 2011; Martell & Shetrone 2013; Adamow et al. 2014) report that some giants with large Li enhancement are occupied between the bump and tip of the RGB. It would be a worthwhile exercise to differentiate RGB stars from the early asymptotic giant branch (AGB) stars. It is well known that many AGB stars produce Li through the Cameron-Fowler mechanism (Cameron & Fowler 1971) in their interiors and gets dredged up to the surface (see Sackmann & Boothroyd 1992).

Acknowledgements. We sincerely thank the referee who made constructive suggestions of using WISE data, which made our interpretations more robust. This study is sponsored by the Chinese Academy of Sciences Visiting Fellowship for Researchers from Developing Countries, Grant No. 2013FFJB0008, and partially supported by the National Natural Science Foundation of China under grants Nos. 11450110404, 11390371, and 11233004. Y.B.K is thankful to T. Medupe for his kind support through NRF grant at NWU. This research made use of the Simbad database and the NASA ADS service.

References

Adamow, M., Niedzielski, A., Villaver, E., Wolszczan, A., & Nowak, G. 2014, A&A, 569, A55
Balachandran, S. C., Fekel, F. C., Henry, G. W., & Uitenbroek, H. 2000, ApJ, 542, 978
Bertelli, G., Girardi, L., Marigo, P., & Nasi, E. 2008, A&A, 484, 815
Bessell, M. S., Castelli, F., & Plez, B. 1998, A&A, 333, 231
Brown, J. A., Sneden, C., Lambert, D. L., & Dutchover, E. J. 1989, ApJS, 71, 293
Cameron, A. G. W., & Fowler, W. A. 1971, ApJ, 164, 111
Carlberg, J. K., Smith, V. V., Cunha, K., Majewski, S. R., & Rood, R. T. 2010, ApJ, 723, L103
Castilho, B. V., Gregorio-Hetem, J., Spite, F., Spite, M., & Barbuy, B. 1998, A&AS, 127, 139
Charbonnel, C., & Balachandran, S. C. 2000, A&A, 359, 563
Cohen, M., Wheaton, W. A., & Megeath, S. T. 2003, AJ, 126, 1090
Cutri, R. M., et al. 2012, VizieR Online Data Catalog: II/311
Cutri, R. M., et al. 2013, VizieR Online Data Catalog: II/328
Cyburt, R. H., Fields, B. D., & Olive, K. A. 2008, J. Cosmology Astropart. Phys., 11, 12
de la Reza, R., & Drake, N. A. 2012, in Circumstellar Dynamics at High Resolution, eds. A. C., Carciofi & T. Rivinius, ASP Conf. Ser., 464, 51
de La Reza, R., Drake, N. A., & da Silva, L. 1996, ApJ, 456, L115
de La Reza, R., Drake, N. A., da Silva, L., Torres, C. A. O., & Martin, E. L. 1997, ApJ, 482, L77
Denissenkov, P. A. 2012, ApJ, 753, L3
Denissenkov, P. A., & Herwig, F. 2004, ApJ, 612, 1081
Drake, N. A., de la Reza, R., da Silva, L., & Lambert, D. L. 2002, AJ, 123, 2703
Egan, M. P., Price, S. D., Kraemer, K. E., et al. 2003, VizieR Online Data Catalog: V/114
Fekel, F. C., & Watson, L. C. 1998, AJ, 116, 2466
Gonzalez, O. A., Zoccali, M., Monaco, L., et al. 2009, A&A, 508, 289
Gratton, R. G., & D'Antona, F. 1989, A&A, 215, 66

Gregorio-Hetem, J., Castilho, B. V., & Barbuy, B. 1993, A&A, 268, L25
Hanni, L. 1984, Sov. Astron. Lett., 10, 51
Harris, M. J., Lambert, D. L., & Smith, V. V. 1988, ApJ, 325, 768
Helou, G., & Walker, D. W. 1988, Infrared astronomical satellite (IRAS) catalogs and atlases, The small scale structure catalog
Iben, I. J. 1967a, ApJ, 147, 650
Iben, I. J. 1967b, ApJ, 147, 624
Ivezic, Z., Nenkova, M., & Elitzur, M. 1999 [arXiv:astro-ph/9910475]
Jasniewicz, G., Parthasarathy, M., de Laverny, P., & Thévenin, F. 1999, A&A, 342, 831
Jura, M. 2003, ApJ, 582, 1032
Kirby, E. N., Fu, X., Guhathakurta, P., & Deng, L. 2012, ApJ, 752, L16
Kleinmann, S. G., Cutri, R. M., Young, E. T., Low, F. J., & Gillett, F. C. 1986, IRAS Serendipitous Survey Catalog (Tucson: Univ. of Arizona)
Kumar, Y. B., & Reddy, B. E. 2009, ApJ, 703, L46
Kumar, Y. B., Reddy, B. E., & Lambert, D. L. 2011, ApJ, 730, L12
Kurucz, R. L. 1994, www.kurucz.harvard.edu
Lebzelter, T., Uttenthaler, S., Busso, M., Schultheis, M., & Aringer, B. 2012, A&A, 538, A36
Lind, K., Asplund, M., & Barklem, P. S. 2009, A&A, 503, 541
Liu, Y. J., Tan, K. F., Wang, L., et al. 2014, ApJ, 785, 94
Luck, R. E., & Heiter, U. 2007, AJ, 133, 2464
Martell, S. L., & Shetrone, M. D. 2013, MNRAS, 430, 611
Matteucci, F. 2010, in IAU Symp. 268, eds. C. Charbonnel, M. Tosi, F. Primas, & C. Chiappini, 453
Mishenina, T. V., Bienaymé, O., Gorbaneva, T. I., et al. 2006, A&A, 456, 1109
Monaco, L., Villanova, S., Moni Bidin, C., et al. 2011, A&A, 529, A90
Monaco, L., Boffin, H. M. J., Bonifacio, P., et al. 2014, A&A, 564, L6
Monet, D. G., Levine, S. E., Canzian, B., et al. 2003, AJ, 125, 984
Moshir, M., Kopan, G., Conrow, T., et al. 1990, BAAS, 22, 1325
Ossenkopf, V., Henning, T., & Mathis, J. S. 1992, A&A, 261, 567
Palacios, A., Charbonnel, C., & Forestini, M. 2001, A&A, 375, L9
Plets, H., Waelkens, C., Oudmaijer, R. D., & Waters, L. B. F. M. 1997, A&A, 323, 513
Reddy, B. E., & Lambert, D. L. 2005, AJ, 129, 2831
Reddy, B. E., Lambert, D. L., Hrivnak, B. J., & Bakker, E. J. 2002, AJ, 123, 1993
Ruchti, G. R., Fulbright, J. P., Wyse, R. F. G., et al. 2011, ApJ, 743, 107
Sackmann, I.-J., & Boothroyd, A. I. 1992, ApJ, 392, L71
Schröder, K., & Cuntz, M. 2005, ApJ, 630, L73
Silva Aguirre, V., Ruchti, G. R., Hekker, S., et al. 2014, ApJ, 784, L16
Skrutskie, M. F., Cutri, R. M., Stiening, R., et al. 2006, AJ, 131, 1163
Strassmeier, K., Washuettl, A., Granzer, T., Scheck, M., & Weber, M. 2000, A&AS, 142, 275
van der Veen, W. E. C. J., & Habing, H. J. 1988, A&A, 194, 125
van Leeuwen, F. 2007, HIPPARCOS, the New Reduction of the Raw Data, Asrtophys. Space Sci. Lib., 350
Wallerstein, G., & Sneden, C. 1982, ApJ, 255, 577
Wright, E. L., Eisenhardt, P. R. M., Mainzer, A. K., et al. 2010, AJ, 140, 1868
Yamamura, I., Makiuti, S., Ikeda, N., et al. 2010, VizieR Online Data Catalog: II/298
Zuckerman, B., Kim, S. S., & Liu, T. 1995, ApJ, 446, L79